2017

Computed tomography and magnetic resonance findings of fat-poor angiomyolipomas

Aaron M. Potretzke
Washington University School of Medicine in St. Louis

Theodora A. Potretzke
Mayo Clinic

Tyler M. Bauman
Washington University School of Medicine in St. Louis

B. Alexander Knight
Washington University School of Medicine in St. Louis

Alyssa M. Park
Washington University School of Medicine in St. Louis

See next page for additional authors

JOURNAL OF ENDOUROLOGY
Volume 31, Number 2, February 2017

Pp. 119–128
DOI: 10.1089/end.2016.0219

Computed Tomography and Magnetic Resonance Findings of Fat-Poor Angiomyolipomas

Aaron M. Potretzke, MD,[1] Theodora A. Potretzke, MD,[2] Tyler M. Bauman, BS,[1] B. Alexander Knight, MD,[1] Alyssa M. Park, MD,[1] Jonathan M. Mobley, MD,[1] Robert Sherburne Figenshau, MD,[1] and Cary Lynn Siegel, MD[3]

ABSTRACT

Introduction: Approximately 5% of angiomyolipomas (AMLs) are classified as ''fat poor'' due to lack of visually detectable fat on imaging, making them difficult to distinguish from renal cell carcinoma. Recent investigations have proposed CT and MR imaging features suggestive of fat-poor AML (fp-AML). Herein, we determined the frequency of these features in a cohort of fp-AMLs by retrospective review of preoperative imaging.
Methods: A pathology database query from January 2005 to August 2013 identified 49 renal specimens of AML with available imaging. A retrospective review of all CT and MR images of these 49 cases was conducted. Cases with visually detectable fat on imaging were excluded.
Results: A total of 26 fp-AMLs were identified. Thirteen lesions had available unenhanced CT images, of which eight (62%) were hyperdense compared to the adjacent renal parenchyma, while five (38%) were isodense. Twenty lesions had enhanced CT images: 14 (70%) and 6 (30%) with homogeneous and heterogeneous enhancement, respectively. Of the nine lesions with enhanced MR sequences, five (56%) were homogeneously enhancing, and four (44%) were heterogeneously enhancing. Eight of nine (89%) lesions had hypointense signal intensity (SI) on T2-weighted MR sequences, while one (11%) had hyperintense SI. None of the eight lesions displayed a decrease in signal on fat-suppressed sequences.
Conclusions: In this study, we confirmed common imaging features of fp-AML: high attenuation on unenhanced CT sequences, homogeneous enhancement on CT, and hypointensity on T2-weighted MR. When these features are present, a renal mass biopsy may be prudent.

Keywords: angiomyolipoma, computed tomography, diagnosis, magnetic resonance, small renal mass

Introduction

Renal angiomyolipoma (AML) represents a relatively rare, benign neoplasm; its prevalence has been reported to be between 0.1% and 2.2%.[1,2] While large (i.e., >4 cm) and symptomatic lesions warrant intervention, smaller lesions are observed.[3] Distinguishing AML from renal cell carcinoma (RCC) typically depends on the presence of macroscopic fat. However, ~4.5% of AMLs lack visually detectable fat on imaging and are therefore considered fat-poor AMLs (fp-AMLs).[4,5] The difficulty in distinguishing these benign lesions from RCC has resulted in unnecessary surgeries, as 8.1% to 32.6% of partial nephrectomies are done for benign disease, with AMLs being found in 18.5% to 43.5% of these cases.[5–8]

Improved radiographic identification of fp-AML could reduce surgeries undertaken for suspicion of malignancy. The CT and MR characteristics of fp-AML have been evaluated in several series, although the reliable distinction of these lesions remains elusive.[4] The objective of this investigation was to evaluate the CT and MR characteristics of pathologically proven fp-AMLs, to identify findings that may suggest AML in otherwise ambiguous cases.

Materials and Methods

Patient and pathologic data

After institutional review board approval, a query of the pathology database for AMLs was conducted from January 1, 2005, to August 1, 2013, and these cases were evaluated for

[1]Division of Urologic Surgery, Washington University School of Medicine, St. Louis, Missouri.
[2]Departmen of Radiology, Mayo Clinic, Rochester, Minnesota.
[3]Mallinckrodt Institute of Radiology, Washington University School of Medicine, St. Louis, Missouri.

available preoperative imaging. Forty-nine patients had pathologically proven AML and available imaging. Patients were excluded who had visually detectable fat on imaging ($n=17$) or lesions too small (<3 mm) to evaluate on preoperative CT or MR ($n=6$). The final cohort consisted of 26 patients, all with single tumors.

Demographic and medical history was recorded, including age, gender, medical history, and source of pathologic specimen. Further pathologic descriptions, such as the predominance of smooth muscle or scant fatty component, were recorded. The percentage of fat was not specified in the pathology report.

Computed tomography

Twenty of the 26 patients underwent a preoperative CT examination. Fifteen CTs were performed at our institution, while six were acquired at outside institutions. Due to the retrospective nature of the study and the inclusion of outside imaging, CT acquisition parameters and protocols were not standardized. One patient underwent two preoperative CT examinations (one with corticomedullary phase only and one with pre- and postcontrast images); therefore, the results of 21 preoperative CTs are presented. All patients had postcontrast imaging available in the corticomedullary phase ($n=8$), the nephrographic phase ($n=4$), or both ($n=9$). Thirteen patients had precontrast imaging available, and three studies included an excretory phase.

Magnetic resonance

Nine of the 26 patients underwent MR examinations (6 MR only, 3 MR in addition to CT). Due to the retrospective nature of the study, MR acquisition parameters and protocols were not standardized. Seven studies were performed at our institution, while two were acquired at outside institutions. All nine MR examinations included T2-weighted and postcontrast sequences. Eight MR examinations included fat-suppressed sequences (both in- and opposed-phase and fat-saturated sequences). Eight MRs included unenhanced, corticomedullary, and nephrographic phases, with five of eight having additional delayed postcontrast phases. One MR was performed only with unenhanced and nephrographic phases.

Image analysis

All CT and MR images were reviewed by one fellowship-trained radiologist (C.S.) with 20 years of experience in genitourinary imaging. Tumor diameter, side, and tumor location (upper pole, interpolar, or lower pole) were recorded. Tumors were labeled exophytic, endophytic, or central. Exophytic lesions were further assessed to see if the lesion was entirely exophytic, possessed a round or angular tumor/parenchymal interface, or a ''mushroom'' extension from the renal border (Fig. 1).[9,10] The presence or absence of calcifications and necrosis on CT and necrosis on MR was recorded. For both CT and MR examinations, manually placed regions of interest (ROIs) on the slice with largest volume of tumor were used for density, signal intensity (SI), and enhancement assessment. Homogeneity of enhancement was assessed by gross visual inspection.

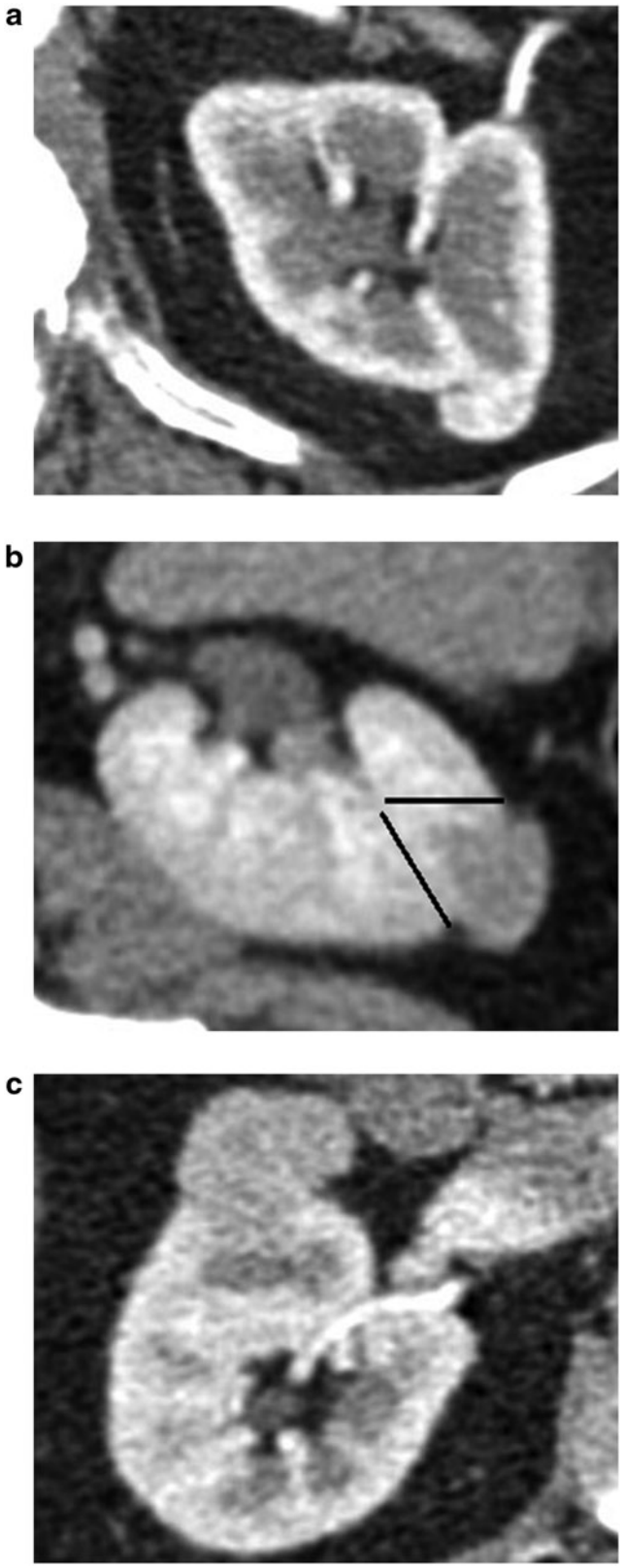

FIG. 1. Examples of radiographic features evaluated in all patients with AML: **(a)** complete exophytic lesion, **(b)** angular interface between tumor and normal renal parenchyma, and **(c)** mushroom-shaped extension beyond the renal border. AML = angiomyolipoma.

CT attenuation was quantitatively measured for renal masses on all phases. Enhancement was defined as an increase in attenuation of 10 HU from the unenhanced to enhanced sequences (either corticomedullary or nephrographic). The attenuation of the tumor was visually compared to the normal renal parenchyma on the unenhanced scans and described as hypodense, isodense, or hyperdense.

On MR, the SI in the tumor on T1- and T2-weighted images was described visually as hypointense, isointense, or hyperintense relative to the adjacent normal renal parenchyma. SI is an arbitrary unit that depends on numerous factors specific to both patient and MRI scanner.[11] These variables include intrinsic properties of T1 and T2 sequences, echo time, inversion time, and rotational angle. The tumor SI on in- and opposed-phase images was recorded with ''SI drop,'' defined as a 10% drop in SI from in-phase to opposed-phase. Lesion SI was measured at the same slice level on in-phase and opposed-phase images with a manually placed round or elliptical ROI. SI values were compared between the two, and a quantitative calculation to assess for signal drop in the opposed phase was performed using the following formula: $(SI_{in}–SI_{opp})/SI_{in} \times 100$, where S_{In} is lesion SI on in-phase images and SI_{opp} is lesion SI on opposed-phase images. The threshold of 10% was chosen to reflect a non-negligible amount of intralesional microscopic fat and to be consistent with prior literature.[12] The SI on fat saturation sequences was visually compared to the same sequence without fat saturation, and the tumor was noted to have or not have macroscopic fat. Quantitative measurements of SI were obtained in each phase. Enhancement was defined as an increase in SI of 10% from precontrast to nephrographic sequences and by using the following equation: % enhancement $= (SI_{post}–SI_{pre})/SI_{pre} \times 100\%$, where SI_{pre} is the precontrast SI of the lesion and SI_{post} is the postcontrast SI of the lesion. A 10% threshold was used to achieve high sensitivity for tumor enhancement and simultaneously avoid artifactual enhancement as can be seen in nonenhancing lesions (e.g., simple cysts may manifest enhancement of 1%–5%).[11]

Descriptive statistics were performed, rather than a formal statistical analysis, given that the aim of the study was to determine frequency of findings.

Table 1. Patient and Gross Tumor Characteristics

Characteristic	
Total number of patients	26
Age	
Mean years ± SD	55 ± 13
Median	54
Gender (%)	
Male	6 (23)
Female	20 (77)
Tuberous sclerosis (%)	
Yes	1 (4)
No	25 (96)
Previous malignancy (%)	
Yes	7 (27)
No	19 (73)
Previous angiomyolipoma (%)	
Yes	1 (4)
No	25 (96)
Symptomatic (%)	
Yes	4 (15)
No	22 (85)
Size (%)	
Mean cm ± SD	1.9 ± 1.0
Median cm (range)	1.5 (0.8–5.3)
Side (%)	
Right	12 (46)
Left	14 (54)
Tumor polarity (%)	
Upper pole	11 (42)
Interpolar	8 (31)
Lower pole	7 (27)
Location (%)	
Exophytic	16 (62)
Endophytic	7 (27)
Central	3 (11)
Completely exophytic (%)	
Yes	3 (12)
No	23 (88)
Mushroom shape/angular interface (%)	
Yes	5 (19)
No	21 (81)

SD = standard deviation.

Table 2. CT Characteristics of Angiomyolipoma with Minimal Fat

Unenhanced CT scans (N = 13)	*Number*	*Percentage (%)*
Attenuation		
Hyperattenuation	8	62
Isoattenuation	5	38
Hypoattenuation	0	0
Enhanced CT scans ($N = 20$)		
Enhancement pattern		
Homogeneous	14	70
Heterogeneous	6	30
Calcifications		
Yes	0	0
No	20	100
Necrosis		
Yes	0	0
No	20	100
Hyperattenuation on unenhanced *or* homogeneous enhancement		
Yes	15	75
No	5	25

Attenuation at each phase	*Mean ± SD*	*Number of CT scans*
Unenchanced, HU	37 ± 10	13
Corticomedullary, HU	116 ± 38	17
Nephrographic, HU	90 ± 27	13
Delayed, HU	55 ± 18	3
Enhancement from unenhanced to		
Corticomedullary, HU	80 ± 45	8
Nephrographic, HU	53 ± 32	10

CT = computed tomography; HU = Hounsfield units.

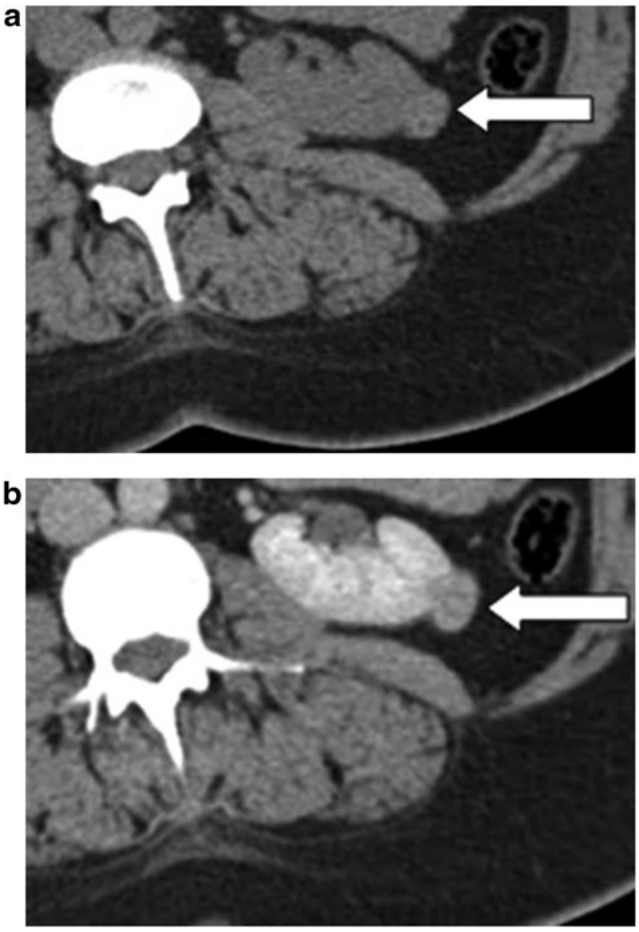

FIG. 2. Transverse CT scan showing a 1.8 cm exophytic, *left lower pole* AML with minimal fat in a 41-year-old female (*arrows*). **(a)** The mass displays hyperattenuation (41 Hounsfield units) compared to the normal renal parenchyma on unenhanced CT. **(b)** The mass exhibits homogeneous enhancement (64 Hounsfield units) in the nephrographic phase. CT = computed tomography.

TABLE 3. MR CHARACTERISTICS OF ANGIOMYOLIPOMA WITH MINIMAL FAT

Characteristic	*Number*	*Percentage (%)*
T1 SI ($N=9$)		
Hyperintense	0	0
Isointense	9	100
Hypointense	0	0
T2 SI ($N=9$)		
Hyperintense	1	11
Isointense	0	0
Hypointense	8	89
In- and opposed-phase SI drop ($N=8$)		
Yes	2	25
No	6	75
Fat saturation ($N=8$)		
Yes	0	0
No	8	100
Enhancement pattern ($N=9$)		
Homogeneous	5	56
Heterogeneous	4	44
Necrosis ($N=9$)		
Yes	0	0
No	9	100
T2 hypointense or homogeneous enhancement ($N=9$)		
Yes	9	100
No	0	0

Characteristic	*Mean ± SD*	*Number of MR sequences*
Unenhanced T1 SI	113 ± 73	9
Corticomedullary T1 SI	227 ± 105	8
Nephrographic T1 SI	229 ± 122	9
Delayed T1 SI	242 ± 65	5
Enhancement from unenhanced to		
Corticomedullary	134 ± 68	8
Nephrographic	108 ± 65	9

SI = signal intensity.

Results

Twenty-three patients were found to have fp-AML after undergoing a partial nephrectomy, while one patient was diagnosed after radical nephrectomy. Two patients were diagnosed by renal mass biopsy, one of which was performed at the time of cryoablation for suspected RCC. Table 1 summarizes the patients' clinical characteristics. One patient had a history of AML and was also the only patient with tuberous sclerosis. Table 1 also displays radiographic characteristics of the AMLs. Twenty-four of the AMLs were less than 4 cm, leaving only 2 AMLs greater than 4 cm in diameter (4.2 and 5.3 cm, respectively).

Review of pathology reports revealed a specific description of ''minimal fat,'' ''fat-poor,'' or similar terms for 12 of the masses. The remaining 14 masses were identified as being fp-AMLs by the pathologic identification of AML and comparison to the preoperative imaging, which did not reveal macroscopic fat. One tumor was the epithelioid variant of AML.

Table 2 summarizes the CT findings of the 20 patients who underwent CT examination. The mean ± standard deviation (SD) density on unenhanced images was 37 ± 10 HU. The range was from 20 to 54 HU, and no lesions had HU measurements near the −10 HU threshold, which is characteristic of fat.[13] All 13 patients with unenhanced and enhanced sequences demonstrated enhancement. Figure 2 illustrates the unenhanced and enhanced CT features of the majority of fp-AMLs.

Table 3 shows the MR characteristics of nine AML lesions. The mean SI ± SD on T1-weighted images before gadolinium was 113 (±73). Enhancement following administration of gadolinium occurred in all cases with available pre- and postgadolinium images. All nine lesions were either hypointense on T2-weighted MR or homogenously enhancing. Figure 3 illustrates common MR features of fp-AMLs.

Discussion

Differentiating an fp-AML from RCC remains challenging, despite improvements in imaging.[4,10] The body of literature describing findings and techniques that may be used to distinguish fp-AMLs is growing (Table 4). Some of the

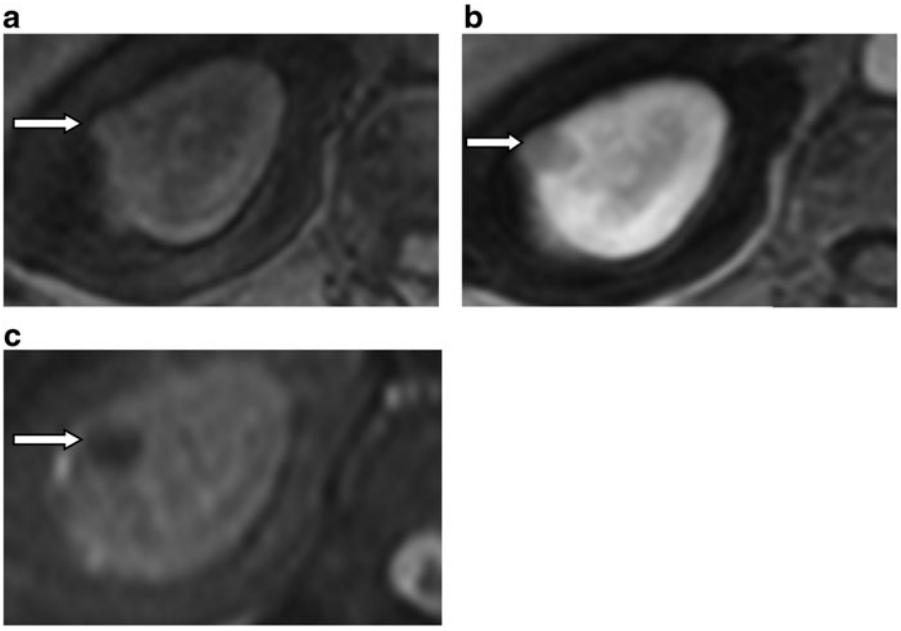

FIG. 3. Transverse MR images showing a 1.1 cm *right upper pole* AML with minimal fat in a 77-year-old female (*arrows*). **(a)** T1-weighted sequence illustrating an isointense mass. **(b)** T1-weighted sequence following gadolinium injection illustrates homogenous enhancement. **(c)** T2-weighted sequence displaying intratumor hypointensity compared to the normal renal parenchyma.

most commonly described findings are (1) hyperdensity on unenhanced CT, (2) homogenous enhancement on enhanced CT, and (3) hypointensity of T2-weighted MR. We evaluated the applicability of these imaging characteristics to an institutional cohort of fp-AMLs. Twenty-one of 26 (81%) patients met at least one of the criteria: hyperattenuation on unenhanced CT (8/13 [62%]), homogeneous enhancement on CT (14/20 [70%]), or hypointensity on T2-weighted MR (8/9 [89%]). Other notable findings in the present review include the absence of a signal drop on opposed-phase MR (6/8 [75%]) and homogenous enhancement on enhanced MR (5/9 [56%]). However, these characteristics are not as often detailed in the literature, and may not help distinguish fp-AML from RCC.[12,14]

As in the present study, many previous studies have found that hyperintensity on unenhanced CT[10,12,15–18] and homogenous enhancement on contrasted CT[4,10,15,17] can help to identify fp-AMLs (Table 4). Similarly, there are several reports that describe a hypointense signal for fp-AMLs on T2-weighted MR.[5,12,14,19–22] In a 2016 investigation, Jeong et al. compared 18 fp-AMLs to 155 RCCs. The authors found that the fp-AMLs had an increased tumor–cortex attenuation ratio on unenhanced CT and had a decreased SI of T2-weighted MR.[12] Likewise, in another large series described by Yang et al., 33 fp-AMLs were compared to 102 RCC tumors. The fp-AMLs were found to have a significantly greater rate of unenhanced attenuation of >38.5 HU and enhanced homogeneity.[17] Still other findings have been associated with fp-AML. Renal masses, which have been described as having either an angular interface with the adjacent parenchyma or having a shape resembling an ''ice-cream cone'' or ''mushroom,''[17,23] are more likely to be fp-AML (Fig. 1). Finally, some authors have proposed using positron emission tomography-CT, which has shown early promising results.[24]

Despite the above imaging descriptions, the findings manifest in fp-AMLs can be inconsistent across studies (Table 4). For example, MR with diffusion-weighted imaging presents conflicting results, as one study found a greater apparent diffusion coefficient (ADC)[25] and another a lower ADC relative to RCC.[26] Also, some authors have reported that in- and opposed-phase MR can be utilized to distinguish fp-AMLs,[14] while others have found these sequences unreliable.[12,21,27] Furthermore, the use of CT histogram analysis to predict fp-AML has been met with conflicting results and is not readily utilized.[13,28,29] Finally, while ultrasound provides characteristic findings (i.e., hyperechogenicity) for lipid-rich AMLs, the ultrasonic findings for fp-AML are variable. In the present cohort, seven patients had ultrasounds available for interpretation. Four of the fp-AMLs were hyperechoic, while three were hypoechoic.

The differing quantity of fat in each tumor makes universal findings on imaging unlikely. Thus, it is most likely that no single finding or instrument will be perfectly accurate. Recent work by Kim et al. has suggested a more comprehensive scoring system, which includes both clinical and radiographic variables. The scoring system was able to yield an area under the curve of 0.919. At various cutoff points, the system conferred accuracy, sensitivity, and specificity as high as 90%, 68%, and 95%, respectively.[15] Including multiple variables in such a system is time-consuming, not easily calculable, and presents challenges in any health system, in which imaging protocols are not standardized.

The rate of benign tumor extirpation remains unsatisfactory, and one of the most common benign lesions excised is AML.[5–8] Thus, improved diagnostic practices are necessary. The use of percutaneous biopsy in patients with small renal masses may augment the effectiveness of current management of small renal masses. Contemporary biopsy techniques afford yields of >80% to 90%, benignity versus malignancy accuracy of 74% to 100%, and complications rates of 1% to 2%.[30] Given the safety and accuracy profiles of renal biopsy, it is reasonable to assert that a biopsy should be undertaken in any patient with a radiographic indication of

Table 4. Summary of Select Studies with Radiographic Findings in Fat-Poor Angiomyolipoma

Study				*Radiographic findings*			
Author	Year	Fat-poor AMLs (*N*)	Comparison group (*N*)	Noncontrasted CT findings	Contrasted CT findings	T2 MR findings	In- and opposed-phase MR
Present study	2016	26	NA	Hyperdensity	Homogeneous enhancement	Hypointensity	
Catalano et al.[28]	2008	22	ccRCC (483)	Pixel histogram analysis does not distinguish fp-AML from ccRCC			
Chaudhry et al.[29]	2012	20	ccRCC and papillary RCC (45)	Pixel histogram analysis does not distinguish fp-AML from RCC			
Choi et al.[19]	2011	10	Non-AML (57 RCC +4 oncocytomas)			**fp-AMLs are hypointense relative to non-AML (AUC of ROC curve = 0.926)**	
Chung et al.[20]	2014	22	Non-AML (86 RCC, 2 oncocytomas, 1 carcinoid tumor)			**Fat-suppressed T2 images using tumor-to-kidney SI can be used to distinguish fp-AML from RCC (98% of tumors with ratio >1.09 were RCC)**	
Ferré et al.[27]	2014	12	Non-AML (95 RCC, 8 oncocytomas, 1 lymphoma, 1 thyroid metastasis)				Double-echo gradient chemical shift MRI is not a confident tool to differentiate renal fp-AMLs from other homogenous renal tumors
Hindman et al.[21]	2012	20	ccRCC (88)			**Low SI relative to renal parenchyma correlates with fp-AML**	Diagnostic accuracy of opposed-phase and in-phase MR of ccRCC vs. fp-AML is poor
Jeong et al.[12]	2016	18	All RCC (155)	**Increased tumor–cortex attenuation differentiated fp-AML from RCC, except chromophobe**		**Decreased tumor–cortex intensity compared to all RCC. Did not differentiate from papillary**	No difference found

(*continued*)

TABLE 4. (CONTINUED)

Study				*Radiographic findings*			
Author	Year	Fat-poor AMLs (*N*)	Comparison group (*N*)	Noncontrasted CT findings	Contrasted CT findings	T2 MR findings	In- and opposed-phase MR
Jhaveri et al.[14]	2014	26	All RCC (71)			**Homogenous low T2 intensity favors fp-AML over RCC**	Percentage SI drop >20% has a high positive predictive value for ccRCC over non-ccRCC and fp-AML
Jinzaki et al. [10]	1997	6	All RCC (100)	**Homogenous high attenuation is suggestive of fp-AML**	**Homogenous enhancement with contrast is suggestive of fp-AML**		
Kim MH et al.[15]	2013	48	All RCC (359)	**Hyperdense compared to all RCC and RCC subtypes**	**Homogenous enhancement compared to all RCC.** A multidetector CT scoring system can distinguish fp-AML from RCC		
Kim JY et al.[13]	2008	34	All RCC (110)	Histogram analysis able to distinguish fp-AML from RCC			
Kim KH et al.[23]	2013	18	All RCC (135)	Ice-cream cone shape and small tumor size predict fp-AML			
Kim JK et al.[4]	2004	19	All RCC (62)		**Homogeneous tumor enhancement and prolonged enhancement pattern can help differentiate fp-AML from RCC**		
Mytsyk et al.[25]	2014	5	ccRCC (and oncocytoma) (19)			The apparent diffusion coefficient is higher in AML than ccRCC	
Sasamori et al.[26]	2014	4	Other renal masses (27)			The apparent diffusion coefficient is lower in AML than ccRCC	
Sasiwimonphan et al.[5]	2012	15	All RCC (104)			**fp-AML has a lower T2 SI ratio than RCC**	fp-AML has a higher SI index ratio than RCC

(*continued*)

TABLE 4. (CONTINUED)

Study				*Radiographic findings*			
Author	Year	Fat-poor AMLs (*N*)	Comparison group (*N*)	Noncontrasted CT findings	Contrasted CT findings	T2 MR findings	In- and opposed-phase MR
Schieda et al.[22]	2015	10	All RCC (77)			**Hypointense compared to ccRCC and chromophobe, but not papillary**	
Woo et al.[16]	2014	24	Non-ccRCC (55)	**Hyperdense compared to non-ccRCC**	A classification and regression tree analysis-based algorithm can predict fp-AML		
Yang et al.[17]	2013	33	All RCC (102)	**Unenhanced attenuation >38.5 HU**	Angular interface, hypodense rim, **homogeneous enhancement** can differentiate fp-AML from RCC		
Zhang et al.[18]	2013	21	Papillary RCC (23)	**Hyperdense compared to papillary RCC**	Intratumoral vessels and hyperdensity associated with fp-AML, compared to papillary RCC		

Bolded text indicates study finds consistent with the results of the current study.

AML = angiomyolipoma; AUC = area under the curve; ccRCC = clear cell renal-cell carcinoma; fp-AML = fat-poor AML; NA = not applicable; RCC = renal-cell carcinoma; ROC = receiver operating characteristic.

possible benignity, or for any patient for whom the management may change based on biopsy results.

There are limitations to the present study, many of which are attributable to its retrospective nature. First, there was variability present in the imaging protocols. Furthermore, the series of cases is small, although there are few series with a larger cohort of fp-AMLs. A number of AMLs were not included in the present description due to the lack of available outside imaging. Also, diffusion-weighted MR imaging and CT histogram analysis were not available for many of the patients in this cohort, making comparison to the findings of previous reports impossible. In addition, all of the imaging was interpreted by a single, genitourinary-dedicated, fellowship-trained radiologist; however, she was not blinded to the diagnosis of fp-AML. Importantly, the present cohort was not matched to a group of similar non-fp-AMLs (e.g., RCCs), which prohibits statistical conclusions. Future work on fp-AMLs should seek to standardize imaging protocols and increase patient cohorts through multi-institutional collaborations. Finally, future investigations may benefit from focus on the inclusion of clinical variables (e.g., female gender) and novel techniques to improve the prospective identification of fp-AMLs.

Conclusion

The distinction between fp-AML and RCC continues to be difficult and may result in unnecessary interventions for these benign lesions. In this series, the majority of fp-AMLs were found in young females with asymptomatic, small renal masses. The presence of a small renal mass with hyperattenuation compared to normal renal parenchyma on unenhanced CT, homogeneous enhancement on enhanced CT, and a hypointense SI compared to normal renal parenchyma on T2-weighted MR should raise the suspicion of an fp-AML. Performing a renal mass biopsy when these features are present may confirm the diagnosis of AML and prevent unnecessary treatment of these benign tumors.

Author Disclosure Statement

No competing financial interests exist.

References

1. Fujii Y, Ajima J, Oka K, Tosaka A, Takehara Y. Benign renal tumors detected among healthy adults by abdominal ultrasonography. Eur Urol 1995;27:124–127.
2. Rule AD, Sasiwimonphan K, Lieske JC, Keddis MT, Torres VE, Vrtiska TJ. Characteristics of renal cystic and solid lesions based on contrast-enhanced computed tomography of potential kidney donors. Am J Kidney Dis 2012;59:611–618.
3. Flum AS, Hamoui N, Said MA, et al. Update on the diagnosis and management of renal angiomyolipoma. J Urol 2016;195:834–846.
4. Kim JK, Park SY, Shon JH, Cho KS. Angiomyolipoma with minimal fat: Differentiation from renal cell carcinoma at biphasic helical CT. Radiology 2004;230:677–684.
5. Sasiwimonphan K, Takahashi N, Leibovich BC, Carter RE, Atwell TD, Kawashima A. Small (<4 cm) renal mass: Differentiation of angiomyolipoma without visible fat from renal cell carcinoma utilizing MR imaging. Radiology 2012;263:160–168.
6. Jeon HG, Lee SR, Kim KH, et al. Benign lesions after partial nephrectomy for presumed renal cell carcinoma in masses 4 cm or less: Prevalence and predictors in Korean patients. Urology 2010;76:574–579.
7. Fujita T, Iwamura M, Wakatabe Y, et al. Predictors of benign histology in clinical T1a renal cell carcinoma tumors undergoing partial nephrectomy. Int J Urol 2014;21: 100–102.
8. Schachter LR, Cookson MS, Chang SS, et al. Second prize: Frequency of benign renal cortical tumors and histologic subtypes based on size in a contemporary series: What to tell our patients. J Endourol 2007;21:819–823.
9. Verma SK, Mitchell DG, Yang R, et al. Exophytic renal masses: Angular interface with renal parenchyma for distinguishing benign from malignant lesions at MR imaging. Radiology 2010;255:501–507.
10. Jinzaki M, Tanimoto A, Narimatsu Y, et al. Angiomyolipoma: Imaging findings in lesions with minimal fat. Radiology 1997;205:497–502.
11. Ho VB, Allen SF, Hood MN, Choyke PL. Renal masses: Quantitative assessment of enhancement with dynamic MR imaging. Radiology 2002;224:695–700.
12. Jeong CJ, Park BK, Park JJ, Kim CK. Unenhanced CT and MRI parameters that can be used to reliably predict fat-invisible angiomyolipoma. Am J Roentgenol 2016;206: 340–347.
13. Kim JY, Kim JK, Kim N, Cho KS. CT histogram analysis: Differentiation of angiomyolipoma without visible fat from renal cell carcinoma at CT imaging. Radiology 2008;246: 472–479.
14. Jhaveri KS, Elmi A, Hosseini-Nik H, et al. Predictive value of chemical-Shift MRI in distinguishing clear cell renal cell carcinoma from non-clear cell renal cell carcinoma and minimal-fat angiomyolipoma. Am J Roentgenol 2015;205: W79–W86.
15. Kim MH, Lee J, Cho G, Cho KS, Kim J, Kim JK. MDCT-based scoring system for differentiating angiomyolipoma with minimal fat from renal cell carcinoma. Acta Radiol 2013;54:1201–1209.
16. Woo S, Cho JY, Kim SH, Kim SY. Angiomyolipoma with minimal fat and non-clear cell renal cell carcinoma: Differentiation on MDCT using classification and regression tree analysis-based algorithm. Acta Radiol 2014;55: 1258–1269.
17. Yang CW, Shen SH, Chang YH, et al. Are there useful CT features to differentiate renal cell carcinoma from lipid-poor renal angiomyolipoma? Am J Roentgenol 2013;201: 1017–1028.
18. Zhang YY, Luo S, Liu Y, Xu RT. Angiomyolipoma with minimal fat: Differentiation from papillary renal cell carcinoma by helical CT. Clin Radiol 2013;68:365–370.
19. Choi HJ, Kim JK, Ahn H, Kim CS, Kim MH, Cho KS. Value of T2-weighted MR imaging in differentiating low-fat renal angiomyolipomas from other renal tumors. Acta Radiol 2011;52:349–353.
20. Chung MS, Choi HJ, Kim MH, Cho KS. Comparison of T2-weighted MRI with and without fat suppression for differentiating renal angiomyolipomas without visible fat from other renal tumors. Am J Roentgenol 2014;202:765–771.
21. Hindman N, Ngo L, Genega EM, et al. Angiomyolipoma with minimal fat: Can it be differentiated from clear cell

renal cell carcinoma by using standard MR techniques? Radiology 2012;265:468–477.
22. Schieda N, Dilauro M, Moosavi B, et al. MRI evaluation of small (<4 cm) solid renal masses: Multivariate modeling improves diagnostic accuracy for angiomyolipoma without visible fat compared to univariate analysis. Eur Radiol 2015;26:2242–2251.
23. Kim KH, Yun BH, Jung SI, et al. Usefulness of the ice-cream cone pattern in computed tomography for prediction of angiomyolipoma in patients with a small renal mass. Korean J Urol 2013;54:504–509.
24. Ho CL, Chen S, Ho KM, et al. Dual-tracer PET/CT in renal angiomyolipoma and subtypes of renal cell carcinoma. Clin Nucl Med 2012;37:1075–1082.
25. Mytsyk Y, Borys Y, Komnatska I, Dutka I, Shatynska-Mytsyk I. Value of the diffusion-weighted MRI in the differential diagnostics of malignant and benign kidney neoplasms—our clinical experience. Pol J Radiol 2014;79:290–295.
26. Sasamori H, Saiki M, Suyama J, Ohgiya Y, Hirose M, Gokan T. Utility of apparent diffusion coefficients in the evaluation of solid renal tumors at 3T. Magn Reson Med Sci 2014;13:89–95.
27. Ferre R, Cornelis F, Verkarre V, et al. Double-echo gradient chemical shift MR imaging fails to differentiate minimal fat renal angiomyolipomas from other homogeneous solid renal tumors. Eur J Radiol 2015;84:360–365.
28. Catalano OA, Samir AE, Sahani DV, Hahn PF. Pixel distribution analysis: Can it be used to distinguish clear cell carcinomas from angiomyolipomas with minimal fat? Radiology 2008;247:738–746.
29. Chaudhry HS, Davenport MS, Nieman CM, Ho LM, Neville AM. Histogram analysis of small solid renal masses: Differentiating minimal fat angiomyolipoma from renal cell carcinoma. Am J Roentgenol 2012;198:377–383.
30. Prince J, Bultman E, Hinshaw L, et al. Patient and tumor characteristics can predict nondiagnostic renal mass biopsy findings. J Urol 2015;193:1899–1904.

Address correspondence to:
Aaron Potretzke, MD
Division of Urologic Surgery
Washington University School of Medicine
4960 Children's Place
Campus Box 8242
St. Louis, MO 63110

E-mail: potretzke.aaron@mayo.edu

Abbreviations Used

ADC = apparent diffusion coefficient
AML = angiomyolipoma
AUC = area under the curve
ccRCC = clear cell renal-cell carcinoma
CT = computed tomography
fp-AML = fat-poor angiomyolipoma
HU = Hounsfield units
MR = magnetic resonance
RCC = renal-cell carcinoma
ROC = receiver operating characteristic
ROI = region of interest
SI = signal intensity
SI_{in} = lesion signal intensity on in-phase images
SI_{opp} = lesion signal intensity on opposed-phase images
SI_{post} = postcontrast signal intensity
SI_{pre} = precontrast signal intensity